12-Element SIW MIMO Antenna With an Integrated Self-Triplexing System for Advanced Wireless Services

Neeraj Gautam, *Student Member, IEEE,* Kundan Kumar, *Senior Member, IEEE,* Lakhindar Murmu, *Member, IEEE,* and Bipin Chandra Mandi, *Senior Member, IEEE*

***Abstract*—This article introduces a novel 12-element MIMO antenna with an integrated self-triplexing system using a substrate-integrated waveguide for advanced wireless communication services. This antenna comprises 12-stepped shaped radiators within a SIW square cavity, each with an individual 50Ω inset-fed line to excite its corresponding radiator. 12-radiators are arranged into three groups with different radiator sizes to achieve self-triplexing operation. Each group contains four identical radiating elements to function as a MIMO antenna system. The proposed integrated MIMO antenna triplexer operates at three distinct frequencies: 4.49 GHz, 6 GHz, and 6.72 GHz, respectively. The antenna is fabricated on a single-layer substrate to validate its performance. The mutual coupling among any radiator is maintained at less than -22.5 dB within the -10 dB impedance bandwidth (IBW). The gain of the proposed antenna is 4.11 dBi, 4.93 dBi, and 6.20 dBi at the respective frequencies. The proposed antenna has an envelope correlation coefficient (ECC) of less than 0.03 at 4.49 GHz, 0.002 at 6 GHz, and 6.72 GHz, with a diversity gain of more than 9.99 dB across all bands. This antenna eliminates the need for additional signal-separation circuits in multi-band MIMO systems due to its inherent band-separation capability.**

Link to graphical and video abstracts, and to code:
https://latamt.ieeer9.org/index.php/transactions/article/view/10299

***Index Terms*—MIMO antenna, integrated self-triplexer MIMO antenna (ISTMA), isolation, substrate integrated waveguide.**

I. Introduction

In recent years, multiple-input multiple-output (MIMO) communication systems have gained a lot of attention due to their ability to overcome shadowing and fading phenomena in multipath environments [1], [2]. It enhances channel capacity while operating within power and bandwidth limitations for various applications [3]. In MIMO configurations, having more antenna elements at the transmitter and receiver ends improves spectral efficiency [4], energy efficiency through beamforming [5], and robustness against fast fading [1]. This advantage arises because the smallest number of antennas at the transmission and reception locations is directly correlated with the channel capacity of an independent identically distributed (i.i.d.) Rayleigh fading MIMO channel [6]–[8]. The advent of heterogeneous networks (HetNets) marks a pivotal shift in advanced wireless communication architectures , enabling the coexistence of multiple wireless technologies [9], [10]. This development allows users to select connectivity options based on environmental conditions and specific application requirements. HetNets are fundamentally supported by critical technologies such as Worldwide Interoperability for Wireless LAN (WLAN), which is valued for its sustainability, cost-effectiveness, well-established infrastructure, and ability to support high data-rate wireless communications [11]–[13]. Globally, WLAN manages localized, high-frequency traffic, optimizing network resources to meet the real-time requirements of various advanced wireless applications in domains such as smart cities, smart homes, and intelligent vehicles. Fig. 1(a) and (b) provide a schematic illustration of an advanced wireless MIMO communication services topology with and without IST (Integrated Self-Triplexing).

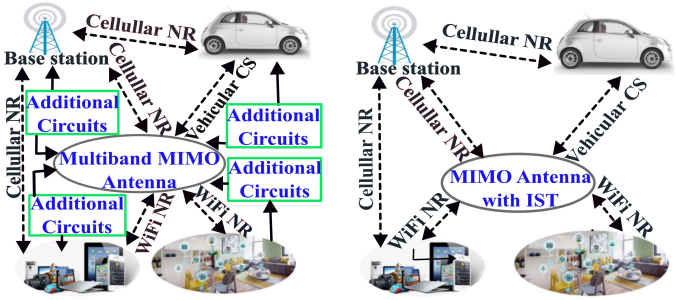

Fig. 1. (a) and (b) are topologies of multi-band MIMO antennas and MIMO antennas with IST connections of smart wireless networks to facilitate seamless connection.

The performance of MIMO wireless communication systems is enhanced by integrating a larger number of miniaturized antenna elements at the transmitter and receiver terminals in a smaller size. Thus, researchers from around the globe are working to integrate a greater number of small antenna elements into MIMO systems while maintaining low mutual coupling and ECC within the given space constraints. This challenging problem has therefore attracted significant research attention.

On the other hand, substrate-integrated waveguide (SIW)

The associate editor coordinating the review of this manuscript and approving it for publication was Roberto S. Murphy (*Corresponding author: Neeraj Gautam*).

Neeraj Gautam, L. Murmu, and B. C. Mandi are in the Department of Electronics and Communication Engineering, International Institute of Information Technology, Naya Raipur, CG 493661, India (e-mails: neeraj@iiitnr.edu.in, lakhindar@iiitnr.edu.in, and bipin@iiitnr.edu.in).

K. Kumar is in the Department of Electronics and Communication Engineering, Dr B R Ambedkar National Institute of Technology, Jalandhar, Punjab, India-144008, India (e-mail: kumarkundan@nitj.ac.in).

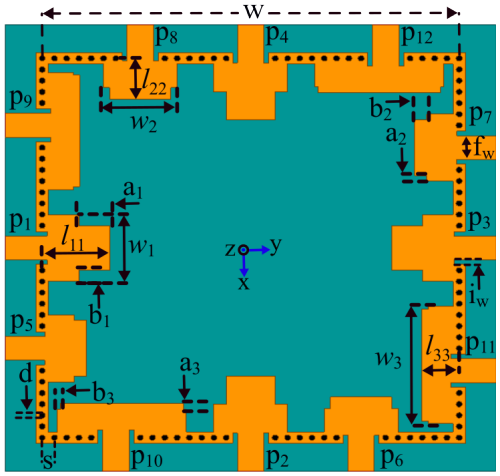

Fig. 2. Layout of the proposed MIMO antenna triplexer. [w = 68, l_{11} = 11, w_1 = 12, a_1 = 5, b_1 = 2, l_{22} = 7.25, w_2 = 12, a_2 = 1, b_2 = 2, l_{33} = 6.1, w_3 = 21, a_3 = 1, b_3 = 0.5, i_w = 0.8, f_W = 4.283, s = 1.5, d = 1 (all in mm)].

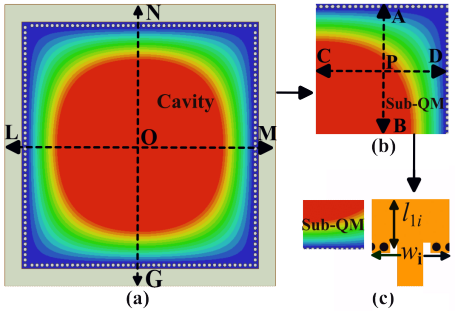

Fig. 3. E-field distribution in (a) Full cavity of SIW, (b) Quarter-mode cavity, and (c) Geometry of a single radiating element of the SIW cavity resonator.

cavity-based antennas offer significant size reduction by employing fractional-mode SIWs such as half-mode (HM), quarter-mode (QM), and related variations [14], [15]. In addition, SIW cavities are known for their low profile, low loss, high quality factor, good radiation performance, simple integration, and offering built-in electrical shielding capabilities [16].

Researchers have developed several multiport MIMO antennas using SIW techniques [17]–[21]. A 4-port MIMO design employing four full-mode SIW cavity-backed slot antennas [17]. In [18], four QM subcavities are used in the 4-port MIMO design, while four full-mode rectangular cavity-based antennas are used in the design of the 4-port MIMO system [19]. In addition, [20], [21] covers 2-port and 4-port MIMO antennas based on TM^z_{010} eighth mode (8M). Due to intrinsic constraints in the HM, QM, and 8M designs, the configurations of these SIW cavity-based MIMO antennas are usually limited to two or four ports. These limits are mostly related to achieving an aperture (the longitudinal wall or border without vias) necessary for radiation. Rotational symmetry has been investigated to allow for the packing of multiple antennas in small places. Numerous rotationally symmetric MIMO antennas with three or four ports have been reported in [22]–[26]. Interestingly, a SIW horn-based array antenna that achieves end-fire radiation is covered in [27] and makes use of an electrically thick substrate ($0.14\lambda_0$). Various researchers worldwide have attempted to develop MIMO systems with a greater number of antenna elements using microstrip or coplanar waveguide technologies [28], [29]. However, these antennas suffer from high losses, low gain, poor front-to-back ratio, unwanted radiation, and electromagnetic interference with nearby components, which limits the performance of advanced wireless communication systems. In [30] antenna employs eight modified U-shaped slots arranged in a 2 × 4 array on the top surface of a substrate integrated waveguide (SIW) cavity. Additionally, all these MIMO antennas operate at a single frequency band. For the multiband MIMO communication systems, a few dual-band/triple-band SIW MIMO antennas have been reported [31], [32]. Furthermore, a small RF front-end transceiver for transmitting and receiving channels on a single panel is essential for recent advanced wireless communication services. Henceforth, multiple radiating elements work in tandem for both the transmitter and the receiver, without interfering with each other. Because of their intrinsic isolation, antenna multiplexers play a crucial role in this scenario by eliminating the use of additional filter/diplexer circuits. Self-diplexing and self-triplexing antennas have been reported in [33], [34]. However, the antennas reported in [33], [34] do not support MIMO system functionality. Only a few studies have reported the integration of MIMO antennas with self-diplexers [35]–[37]. However, [35]–[37] are limited to two frequencies and a 2 × 2 element MIMO antenna with a larger size. To accommodate more frequency bands, a four-element MIMO antenna with an integrated self-triplexer is not presented in the open literature.

This paper presents a novel design of a 12-element SIW MIMO antenna with an integrated self-triplexing system for advanced wireless communication services, such as WLAN, vehicular communication systems (including MIMO-based video transmission applications or robust Wi-Fi connectivity in unmanned aerial vehicles (UAVs)), and the Super Extended C-band at the appropriate frequency band. This antenna comprises 12-stepped shaped radiators within a SIW square cavity. Each radiator is backed by a sub-quarter-mode cavity and excited by 50Ω inset-fed lines. All the radiators are arranged into three groups with different radiator sizes to achieve self-triplexing operation. Each group contains four identical radiating elements to function as a MIMO antenna system. The proposed integrated MIMO antenna triplexer operates at three distinct frequencies: 4.49 GHz, 6 GHz, and 6.72 GHz, respectively. The proposed antenna provides high gain, low mutual coupling, and low ECC, along with a directed radiation pattern and self-shielding using cavity-supported stepped radiators on SIW cavities. The proposed MIMO antenna with an integrated self-triplexer does not require extra filter/diplexer circuits to separate the signal in multi-band MIMO systems due to its inherent band-separation capability. Thus, this antenna can enhance its capacity to mitigate multipath and intermodal interference. This antenna has a broad range of frequency tuning capability. As per the open literature survey, this is the first 12-element MIMO antenna with an integrated triplexer.

In summary, this work introduces a novel antenna architecture based on SIW technology, which uniquely incorporates a 12-element MIMO system with an integrated self-triplexing mechanism within a single SIW cavity. Unlike previously reported SIW MIMO antennas, which are generally limited to eight ports and depend on external multiplexing networks, the proposed design allows for simultaneous multi-port and multi-band operation without requiring additional filtering or triplexing circuitry. This innovative single-cavity self-triplexing approach significantly reduces system complexity, minimizes the footprint, and lowers insertion loss, while enhancing scalability for high-capacity wireless systems. To the authors' knowledge, this is the first study of an SIW-based antenna that combines a 12-port MIMO configuration with integrated self-triplexing. Therefore, it is a strong candidate for applications in next-generation WLAN, vehicular technology, UAVs, and Super Extended C-band communications.

II. Analysis and Design of the Proposed MIMO Antenna with Integrated Triplexer

The illustration presented in Fig. 2 shows an antenna configuration comprising a square SIW cavity and 12-stepped radiators with the overall size of $1.5\lambda_g \times 1.5\lambda_g$. The cavity is enclosed by rows of metallic vias that function as electric walls. The proposed structure features a single continuous substrate-integrated waveguide (SIW) cavity that is electrically segmented into subcavity regions without physical separation. This segmentation is accomplished by strategically placing slots, stepped radiators, and vias, which help to control the field distribution and resonant behavior locally. 12 independent 50 ohms inset feed lines supply the power to the antenna. To mitigate energy dissipation, it is mandatory to follow the recommended specifications of $0.5s \leq d \leq 0.1\lambda_g$, where s is the spacing between the two vias, d is the diameter of the vias, c is the velocity of light, and λ_g is the guided wavelength [15].

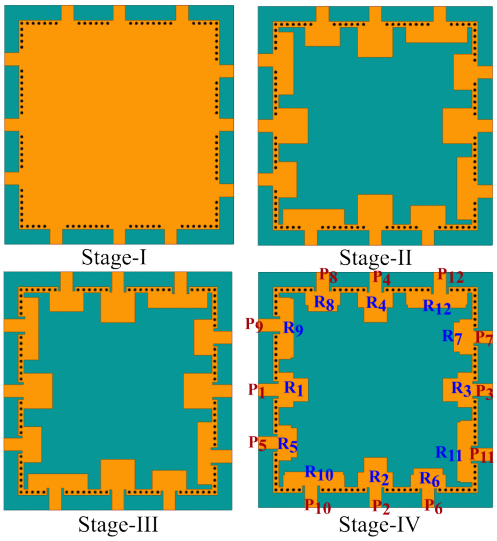

Fig. 4. Development stages: Stage-I involves a full SIW cavity with 12 feeds; Stage-II consists of 12 rectangular resonators; Stage-III features an inset feed; and Stage-IV includes stepped resonators.

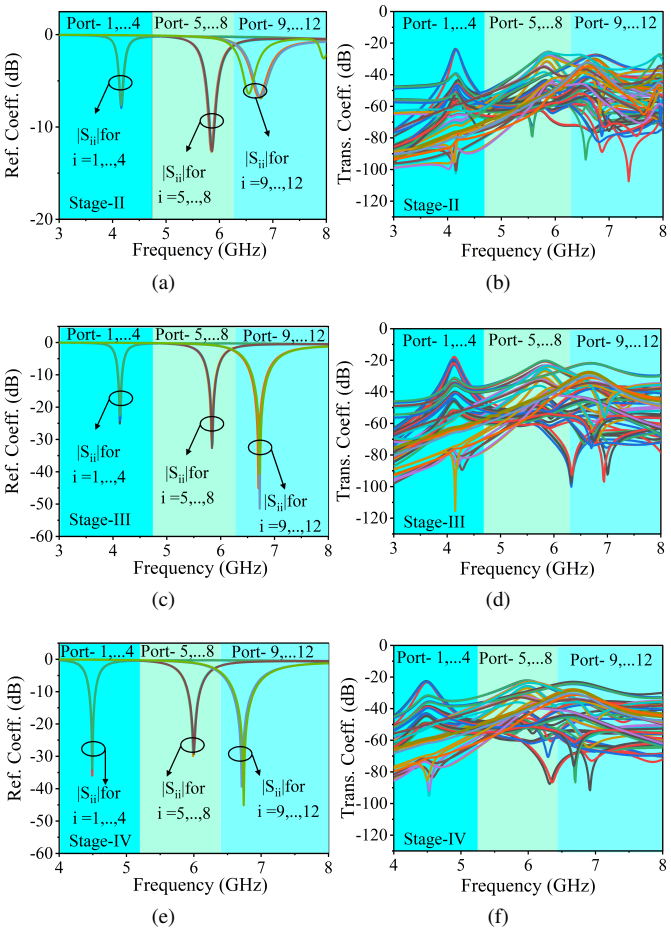

Fig. 5. Development stage results: (a) Stage-II reflection coefficient, (b) Stage-II transmission coefficient, (c) Stage-III reflection coefficient, (d) Stage-III transmission coefficient, (e) Stage-IV reflection coefficient, and (f) Stage-IV transmission coefficient.

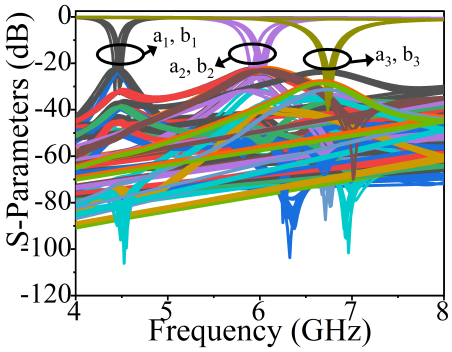

Fig. 6. Parameter variation at different frequencies by varying the length and width of b_1 (1.5 to 2.5 mm), b_2 (1.5 to 2.5 mm), b_3 (0.3 to 0.7 mm), a_1 (4 to 6 mm), a_2 (0.8 to 1.2 mm), and a_3 (0.8 to 1.2 mm).

A. *Design of 12-element MIMO Antenna with Integrated Self-triplexer,*

The antenna is constructed using an SIW cavity, as shown in Fig. 2. Each radiator of the proposed antenna is backed by a sub-quarter-mode cavity. The sub-quarter-mode cavity is created by dividing a full-mode SIW (FMSIW) cavity as

shown in Fig. 3. The FMSIW cavity is divided into four sections by two lines, NG and LM, to create the quarter-mode (QM) cavity as shown in Fig. 3(a). A QM cavity is further divided by two lines, AB and CD, to create the sub-quarter-mode (Sub-QM) cavity as depicted in Fig. 3(b). The individual radiating element is supported by the Sub-QM SIW resonator and fed with a 50-ohm line as shown in Fig. 3(c). The basic dimensions of each radiating is calculated using equation 1 [15].

$$f_{mn0}^{p_i} = \frac{c}{2\pi\sqrt{\varepsilon_{eff}}}\sqrt{\left(\frac{m\pi}{4w_i}\right)^2 + \left(\frac{n\pi}{4l_{1i}}\right)^2} \quad (1)$$

where i (i = 1,2,... 12) are the ports, m and n are the modes of the cavity, w and l are the width and length of the resonator, ε_{eff} ($\varepsilon_{eff} = (\varepsilon_r + 1)/2$) is the effective permittivity, and ε_r is the relative permittivity of the substrate material. Each radiator supports the perturbed TE_{110} mode of the basic cavity. The value of w_i and l_{1i} should be at least $\lambda_g/2$ ($\lambda_g = \lambda_0/\sqrt{\varepsilon_r}$) and $\lambda_g/4$, respectively, where the guided wavelength is equal to the guided wavelength at the operating frequency. Due to the loading effect, the resonant frequency of the radiator is slightly deviated from the frequency obtained from equation 1. Hence, this equation is used only as an initial design for the radiator. The development of the MIMO antenna with an integrated triplexer involves four stages, as shown in Fig.4.

Starting with stage-I, a basic square SIW cavity is taken and fed by twelve 50 ohms lines. To get the proper radiation, 12-radiator are created on the top of the SIW cavity with distinct lengths and widths of l_{11}, l_{22}, l_{33}, w_1, w_2, and w_3 as shown in stage-II of Fig. 4 and the corresponding results are presented in Fig.5(a) and (b). Each radiator is supported by a sub-QM mode, and its initial dimensions are estimated using equation (1). From Fig.5(a) and (b), it is observed that the reflection coefficients of all the radiators do not meet a satisfactory matching level. To improve the matching of all the radiators, inset-fed lines are introduced, as depicted in stage-III of Fig. 4 and the corresponding results are presented in Fig. 5(c) and (d). Reflection coefficients better than -20 dB are achieved for all the radiators. Furthermore, in stage-IV, a stepped structure is created in each radiator by varying the length of b_1 (1.5 to 2.5 mm), b_2 (1.5 to 2.5 mm), b_3 (0.3 to 0.7 mm), a_1 (4 to 6 mm), a_2 (0.8 to 1.2 mm), and a_3 (0.8 to 1.2 mm) to improve the isolation as depicted in Fig.6. Due to the stepped radiators, the isolation among the radiating elements is improved by 2.89 dB, 3.26 dB, and 3.66 dB, as depicted in Fig. 5(f) for p_1 to p_4, p_5 to p_8, and p_9 to p_{12}, respectively. The radiators R_1, R_2, R_3 and R_4 are operating at frequency 4.49 GHz, the radiators R_5, R_6, R_7 and R_8 are operating at frequency 6 GHz, and the radiators R_9, R_{10}, R_{11} and R_{12} are operating at frequency 6.72 GHz.

B. Electric-field and Current Distribution

Fig. 7(a) and (b) illustrate the distribution of electric field (E-field) and surface current on the radiator by exciting the one port of identical radiators at each operating frequency. Fig. 7(a) shows that most of the E-field is contained within the matching stepped radiators. These findings suggest that each port's electric field has remained largely confined within its radiator and has interacted minimally with the fields of the other ports. This observation validates the design's isolating properties for the ports. The field distribution study also confirmed that each radiator supports the perturbed TE_{110} mode. In Fig. 7(b), it is illustrated that the maximum current density tends to concentrate near the radiators. This accumulation of current is essential for effectively controlling the emission and propagation of electromagnetic waves from the antenna. By analyzing the distribution of current density at different frequencies, it showed the gained insights into how these radiators interact with the electromagnetic field, which is crucial for optimizing antenna performance and improving signal strength. In Fig. 7(c), the first three images show the distribution of the E-field with excitation of all identical radiators at their respective frequencies, and the last image shows the distribution of the E-field when all radiators are excited simultaneously. The vector E-field distributions are plotted in the XY and YZ planes at a height of 0.5 mm above the radiator at the respective operating frequencies, as shown in Fig. 7(d). This field distribution also confirmed that each radiator supports the perturbed TE_{110} mode.

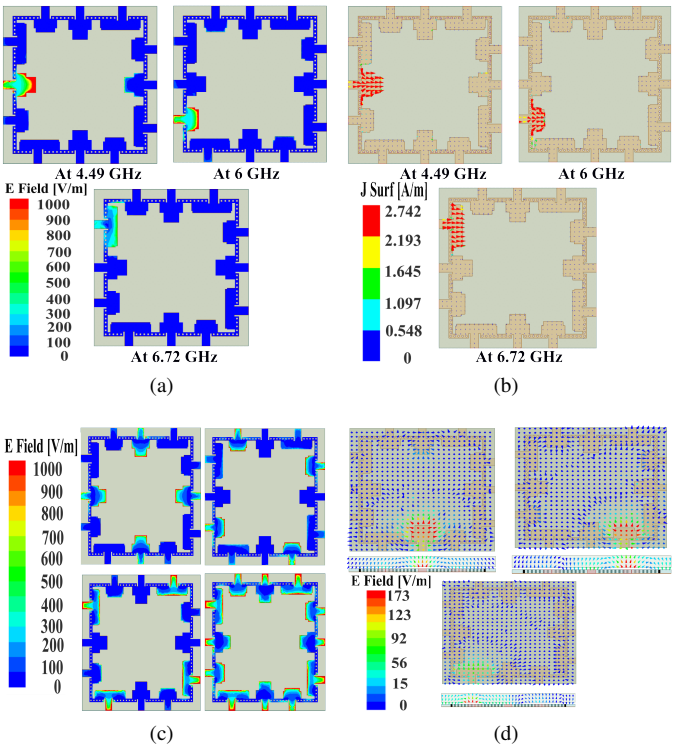

Fig. 7. (a) Electric field, (b) Surface current density distribution at different frequencies when different antenna ports are excited, (c) Multiple ports excited, and (d) Vector E-fields at different frequencies.

C. Equivalent Circuit Model of Proposed ISTMA

The proposed equivalent circuit model for the suggested ISTMA is shown in Fig. 8. A parallel RLC tank circuit is used in this model to represent each cavity resonator, because each SIW cavity behaves as a resonant energy storage

TABLE I
OPTIMIZED COMPONENT VALUES OF PROPOSED ISTMA

Components	Values	Components	Values	Components	Values	Components	Values	Components	Values
$R_1(\Omega)$	48.22	$R_2(\Omega)$	48.21	$R_3(\Omega)$	48.19	$R_4(\Omega)$	48.2	$R_5(\Omega)$	51.12
$R_6(\Omega)$	51.13	$R_7(\Omega)$	51.10	$R_8(\Omega)$	51.11	$R_9(\Omega)$	54.22	$R_{10}(\Omega)$	54.23
$R_{11}(\Omega)$	54.21	$R_{12}(\Omega)$	54.20	L_1(nH)	1.1	L_2(nH)	1.09	L_3(nH)	1.08
L_4(nH)	1.12	L_5(nH)	0.71	L_6(nH)	0.72	L_7(nH)	0.70	L_8(nH)	0.69
L_9(nH)	0.31	L_{10}(nH)	0.32	L_{11}(nH)	0.29	L_{12}(nH)	0.28	C_1(pF)	1.25
C_2(pF)	1.24	C_3(pF)	1.23	C_4(pF)	1.22	C_5(pF)	0.98	C_6(pF)	0.99
C_7(pF)	0.98	C_8(pF)	0.97	C_9(pF)	0.76	C_{10}(pF)	0.75	C_{11}(pF)	0.77
C_{12}(pF)	0.75	K_{15}	0.19	K_{19}	0.29	K_{26}	0.19	K_{210}	0.29
K_{37}	0.19	K_{311}	0.29	K_{48}	0.19	K_{412}	0.29	K_{510}	0.15
K_{611}	0.15	K_{712}	0.15	K_{89}	0.15				

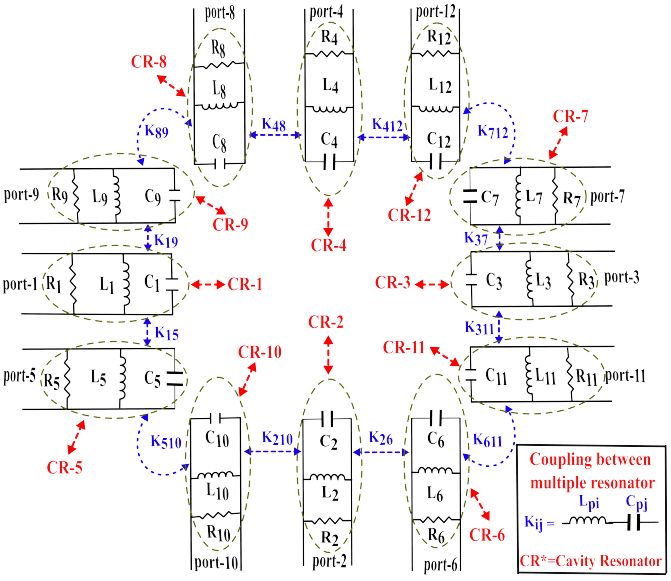

Fig. 8. Model of the proposed multi-element ISTMA's equivalent circuit.

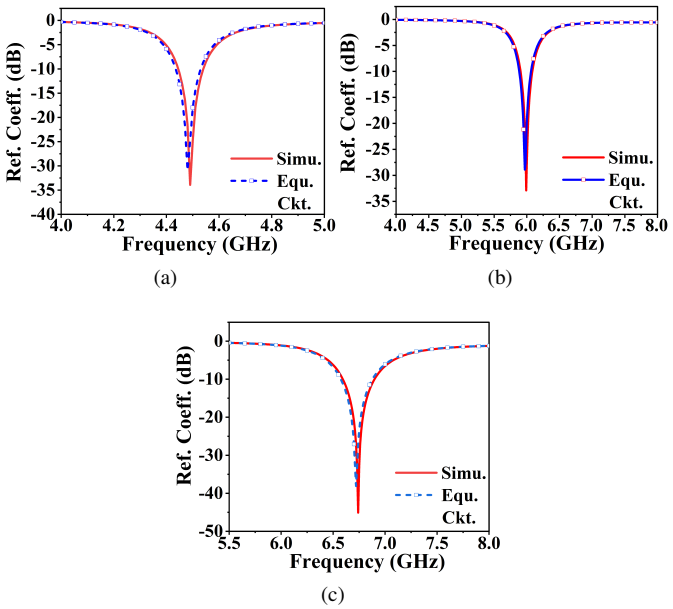

Fig. 9. The results of the EM simulator and equivalent circuit models were compared based on the reflection coefficient: (a) for port-1, (b) for port-5, and (c) for port-9.

structure, which is more accurately represented by a parallel configuration near resonance [37]. Additionally, an L_{pi}, C_{pj} (*i,j* is the port no. from 1 to 12) tuned circuit imitates the parameter K_{ij} (i is not equal to j), which describes the coupling between the multiple cavity resonators. The LC coupling circuit comprises a sequence of connections between the ports that are meticulously calibrated to optimize inter-port isolation. The angular frequency (w_r) and resonant frequency (f_r) of the resonators can be determined using equation 2, while the input impedance (Z_{input}) is derived from equation 3 [37]. This process is essential for analyzing the performance characteristics of the resonators.

$$f_r = \frac{1}{2\pi\sqrt{L_{pi}C_{pj}}} \tag{2}$$

$$Z_{\text{input}} = \frac{jw_rL_{pi}}{1 - w_r^2C_{pj}L_{pi}} \tag{3}$$

The Keysight Advanced Design System (ADS) software has been used to validate the equivalent circuit model of the proposed ISTMA. Table I provides the optimized component values. Additionally, for the suggested ISTMA, Fig. 9 contrasts the reflection coefficient acquired from the electromagnetic (EM) simulation with those obtained from the circuit simulation. The parameters of the first resonator's inductance, resistance, and capacitance are represented by L_1, R_1, and C_1, which can be calculated using ADS. In contrast, the second resonators are represented by L_2, R_2, and C_2, likewise, for all the ports. L_{pi} and C_{pj}, respectively, model the coupling between the multiple resonators.

The above studies have been carried out with the following design guidelines:

1) Design a basic square SIW cavity with 68 x 68 millimeters dimensions.
2) Further, a basic square SIW cavity is divided into twelve stepped patches using metallic vias.
3) The upper part of the cavity traversed variations to stepped patches directed towards each cavity port. The lengths of the radiator were initially determined by calculating the guided wavelength relative to the first resonant frequency, λ_g.
4) To ensure proper matching at all ports, it is recommended to choose a value of mw = 0.004 λ_g for the

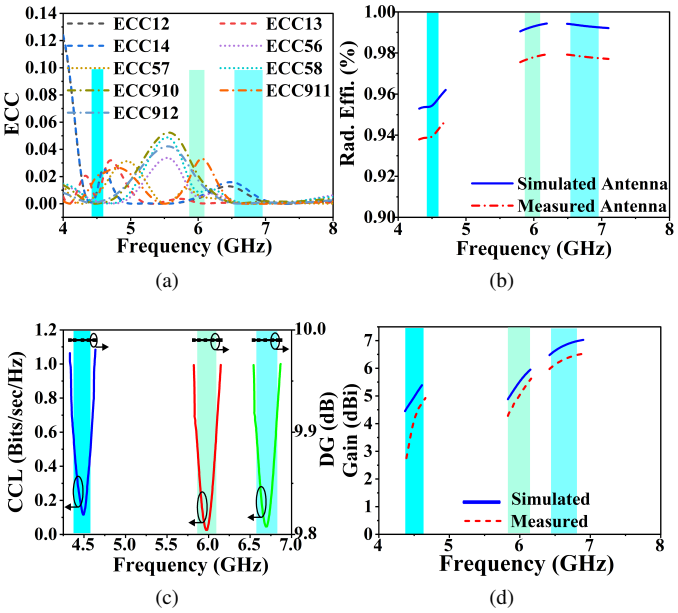

Fig. 10. (a) ECC using radiation patterns for the proposed antennas, (b) Radiation Efficiency, (c) Measured DG and CCL of the proposed antenna, and (d) Gain of the antenna.

matching condition. Furthermore, it is recommended to set λ_g and ml equal to 0.02 λ_g for matching purposes.

5) To enhance the isolation and s-parameters, involve two steps. In the first step, the width and length of each port along the stepped patch have to be varied. This adjustment consists of modifying the exact lengths of patch l_{11} and w_1. In the second step, the patches were used to vary a_1 and b_1 to further improve the isolation.
6) Repeat to obtain other resonance frequencies following Step 5.
7) Implement an integrated twelve-element self-triplexing MIMO antenna using the HFSS simulator and experimentally validate the fabricated prototype.

III. Results and Discussions

A working prototype of a 12-element MIMO antenna with an integrated triplexer (as shown in Fig. 2) is constructed on Rogers RT/duroid 5880 substrates, having tanδ = 0.0009, ε_r = 2.2, and a thickness of 1.57 mm and tested (Fig. 13) to verify the idea. Fig. 12 displays the simulated and measured $|S_{ii}|$ and $|S_{ij}|$ parameters for each radiator. To measure the S-parameters, a Keysight FieldFox Microwave Analyzer (N9916A) is utilized. The measured -10 dB impedance bandwidths for all antennas are obtained as 100 MHz (4.44 to 4.54 GHz), 190 MHz (5.90 to 6.09 GHz), and 330 MHz (6.57 to 6.90 GHz), respectively. From the Fig. 12, it has been seen that the mutual coupling inside the standard bandwidth for every antenna port is less than -22.5 dB. The discrepancy between the simulated and measured S-parameters can be attributed to fabrication tolerances and connector soldering.

The radiation patterns of an identical radiator for ports p_1 to p_{12} in the $\phi = 0°$ and $\phi = 90°$ planes are displayed on the left side (LHS) and right side (RHS) of Fig. 14, at the respective frequencies. A high agreement was found between the measured and simulated radiation patterns. During pattern measurements, only the port in concern is activated; all other ports are terminated with matching loads. In Fig. 10(d), the measured gain of the antenna ranges from 4.11 to 6.20 dBi across the observed bandwidths. The 3D gain pattern is shown in Fig. 11. Table III illustrates the ISTMA far-field performances.

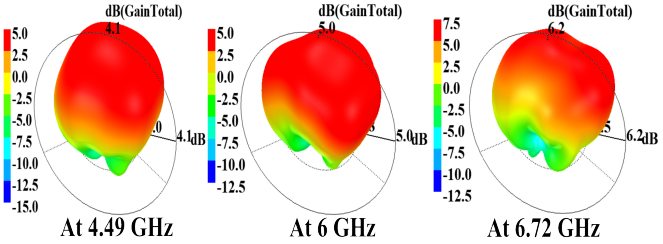

Fig. 11. 3D gain patterns at different frequencies.

Based on the 3-D radiation patterns, it is discovered that the envelope correlation coefficient (ECC) is less than 0.03, 0.002, and 0.002 in the different bandwidths of the antenna ports (4.44 to 4.54 GHz, 5.90 to 6.09 GHz, and 6.57 to 6.90 GHz) [8]. ECC has been calculated using far-field radiation patterns, which provide greater accuracy for multi-port antennas that exhibit complex radiation behavior, as shown in Fig. 10(a) using equation 4. The ECC value can be precisely calculated using scattering parameters, and for even greater accuracy, the far-field pattern method described in [37] offers a superior approach. This method not only enhances the reliability of the results but also elevates the overall clarity of the analysis. Fig. 10(b) depicts radiation efficiency percentages, which are more significant than 94% at each port excited.

$$ECC(\rho_{ij}) = \frac{\left|\iint_0^{4\pi} [\boldsymbol{F}_i(\theta,\Phi) * \boldsymbol{F}_j(\theta,\Phi)]\, d\Omega\right|^2}{\left(\iint_0^{4\pi} |\boldsymbol{F}_i(\theta,\Phi)|^2\, d\Omega \iint_0^{4\pi} |\boldsymbol{F}_j(\theta,\Phi)|^2\, d\Omega\right)} \tag{4}$$

Note: $F_i(\theta)$ and $F_j(\theta)$ (3-D radiation pattern functions) = i^{th} port and j^{th} port are excited, * = Hermitian product, and Ω = solid angle.

Fig. 10(c) illustrates that the CCL (channel capacity loss) of each antenna is less than 0.2 Bits/sec/Hz, using equations 5 and 6, and the diversity gains (DG) are more than 9.99 dB overall in the bands, which is near to the ideal value of 10 dB shown in Fig.10(c), using equation 7 in [38].

$$C_{\text{loss}} = -\log_2 \det\left(\Psi^R\right) \tag{5}$$

where Ψ^R is the matrix that describes the correlation between the elements of the receiving antenna. It can mathematically be defined as follows:

$$\Psi^R = \begin{bmatrix} \Psi_{ii} & \Psi_{ij} \\ \Psi_{ji} & \Psi_{jj} \end{bmatrix} \tag{6}$$

TABLE II
COMPARISON OF THE PROPOSED MIMO ANTENNA'S PERFORMANCE TO OTHER PUBLISHED LITERATURE

Para. / Ref.	Minimum Isolation (dB)	Bandwidth (GHz)	Gain (dBi)	Efficiency (%)	Volume ($\lambda_g{}^3$)	ECC	No. of ports	Antenna topology	Circuit Model
[22]	14	3.3-4.2	6.6	$\geq$ 88	0.2995	$\leq$ 0.05	3	SBNS$^{\#}$	NO
[23]	15	3.3-4.2	N.R.	$\geq$ 88	0.2351	$\leq$ 0.01	3	SBNS$^{\#}$	NO
[24]	13	3.3-5	6.4	$\geq$ 84	0.2351	$\leq$ 0.05	4	SBNS$^{\#}$	NO
[25]	9.5	3.3-4.2	2	$\geq$ 40	0.00235	$\leq$0.06	4	SBNS$^{\#}$	NO
[26]	9.7	3.3-4.2*	0.00416	$\geq$ 36	0.00245	$\leq$0.48	4	SBNS$^{\#}$	NO
[27]	45	27.5-38	9.5	N.R.	N.R.	N.R.	12	SBS$^{\#}$	NO
[28]	20	5.925-6.425	6.7	$\geq$ 86	0.2280	<0.1	8	SBNS$^{\#}$	NO
[29]	10	5.9-7.2	4.1	$\geq$ 62	N.R.	<0.01	8	SBNS$^{\#}$	NO
[30]	28	1.19-1.37	3.68	$\geq$ 85	N.R.	<0.5	8	SBS$^{\#}$	NO
[31]	20	2.3-2.5, 5.15-5.85	5.8	$\geq$ 61	N.R.	<0.004	2	DBS$^{\#}$	NO
[32]	20	3.57, 4.41, 5.43	4.98, 4.6, 3.1	$\geq$ 76, $\geq$ 71.5, $\geq$ 72.8	N.R.	<0.001	2	TBS$^{\#}$	NO
[33]	14	11.05-11.48, 11.4-11.88	6, 5.85	N.R.	N.R.	N.R.	2	SDS$^{\alpha}$	NO
[34]	22.5	7.78–7.99, 9.34–9.53, 9.78–9.96	7.2	$\geq$ 95	N.R.	N.R.	3	STS$^{\alpha}$	NO
[35]	15	4.82-5.46, 5.52-6.21	2.02, 2.96	N.R.	N.R.	$\leq$0.011, $\leq$0.032	4	SDNS$^{\#}$	NO
[36]	23	3.35-3.55, 4.14-4.34	5.35, 6.15	$\geq$ 88, $\geq$ 85	N.R.	$\leq$0.15	4	SDS$^{\#}$	YES
[37]	19	3.5, 5.8	4.77, 5.83	N.R.	N.R.	$\leq$0.00046	4	SDS$^{\#}$	YES
This Work	**22.23, 23.4 25.6**	**4.44-4.54, 5.90-6.09, 6.57-6.90**	**4.11, 4.93, 6.20**	$\geq$ 94, $\geq$ 97, $\geq$ 97	**0.0449**	$\leq$ 0.03, $\leq$ 0.002 $\leq$ 0.002	**12**	**STS$^{\#}$**	**YES**

Note: N.R. = Not Reported, $\star$ = -6 dB reflection, SBNS = Single-band Non SIW, SBS = Single-band SIW, SDS = Self-Diplexing SIW, SDNS = Self-Diplexing Non SIW, STS = Self-Triplexing SIW, DBS = Dual-band SIW, TBS = Triple-band SIW, # = with MIMO and α = without MIMO.

TABLE III
PROPOSED ISTMA PERFORMANCES

Freq. (GHz)	Co-to-X pol (dB)	FTBR (dB)	HPBW (degree)
4.49	$\frac{27.89^{\star}}{42.19^{\#}}$	$\frac{18.61^{\star}}{16.01^{\#}}$	$\frac{89^{\star}}{110^{\#}}$
6	$\frac{18.67^{\star}}{18.09^{\#}}$	$\frac{17.13^{\star}}{15.09^{\#}}$	$\frac{87^{\star}}{142^{\#}}$
6.72	$\frac{22.79^{\star}}{22.59^{\#}}$	$\frac{16.6^{\star}}{17.36^{\#}}$	$\frac{74^{\star}}{140^{\#}}$

Note: # - in ϕ = 90° plane, $\star$ - in ϕ = 0° plane, FTBR = Front-to-back-ratio, HPBW = Half-power Beamwidth.

where,

$$\Psi_{ii} = 1 - \left(|S_{ii}|^2 + |S_{ij}|^2\right)$$
$$\Psi_{jj} = 1 - \left(|S_{jj}|^2 + |S_{ji}|^2\right)$$
$$\Psi_{ij} = -\left(S_{ii}^{*}S_{ij} + S_{ji}^{*}S_{jj}\right)$$
$$\Psi_{ji} = -\left(S_{jj}^{*}S_{ji} + S_{ij}^{*}S_{ii}\right)$$

$$\mathrm{DG} = 10\sqrt{1 - 0.99ECC^2} \tag{7}$$

Mean effective gain (MEG) can operate in the permissible range of -3 dB to -12 dB [38]. With the help of equation 8, the MEG of the respective operating frequencies is -3.39 dB, -3.31 dB, and -3.19 dB.

$$MEG_i = 0.5\eta_{\text{irad}} = 0.5\left(1 - \sum_{j=1}^{N}|S_{ij}|^2\right) \tag{8}$$

where the MEG of a MIMO antenna depends on N, the number of antennas, i is the active antenna, and η_{irad} is the radiation efficiency of the (i^{th}) antenna.

Table II illustrates the comparison of the proposed integrated MIMO antenna triplexer with other reported studies [22]–[37]. Whereas, in [22]–[32] reported the single-band/multi-band-MIMO antennas and in [33], [34], presented the self-diplexer/triplexer antennas. Most reported multi-band MIMO systems do not have the feature of self-band separation. A MIMO antenna configuration with integrated self-diplexing is presented in [35]–[37], featuring self-band-separation, but it is limited to a maximum of two operating bands with a two-identically radiating element MIMO configuration. The proposed design shows compactness, superior gain, increased bandwidth, enhanced efficiency, favourable ECC values, more ports, and an inherent self-band-separation capability of up to three bands with a four-identical radiating-element MIMO configuration.

IV. CONCLUSION

In this paper, a novel, compact, low-profile 12-element SIW MIMO antenna with an integrated self-triplexer is presented for wireless services. The proposed antenna comprises 12-stepped shaped radiators within a SIW square cavity, and each radiator is backed by a sub-quarter-mode cavity. The measured -10 dB IBWs are obtained over more than 100 MHz with better than 94% antenna efficiency over the operational bandwidth. The measured diversity gain and channel capacity loss are found to be 9.99 dB and 0.02 bits/Hz/s, respectively, with a minimum envelope correlation coefficient of 0.03 for 4.49 GHz, 0.002 for 6 GHz, and 6.72 GHz. The proposed SIW MIMO antenna with integrated self-triplexer is suitable for advanced wireless communication services, such as WLAN, vehicular communication systems (MIMO-based video transmitting applications or robust Wi-Fi connectivity in unmanned aerial vehicles (UAVs)), and Super Extended C-band for applications across the wireless environment due to its inherent band-separation capability without the use of additional circuits.

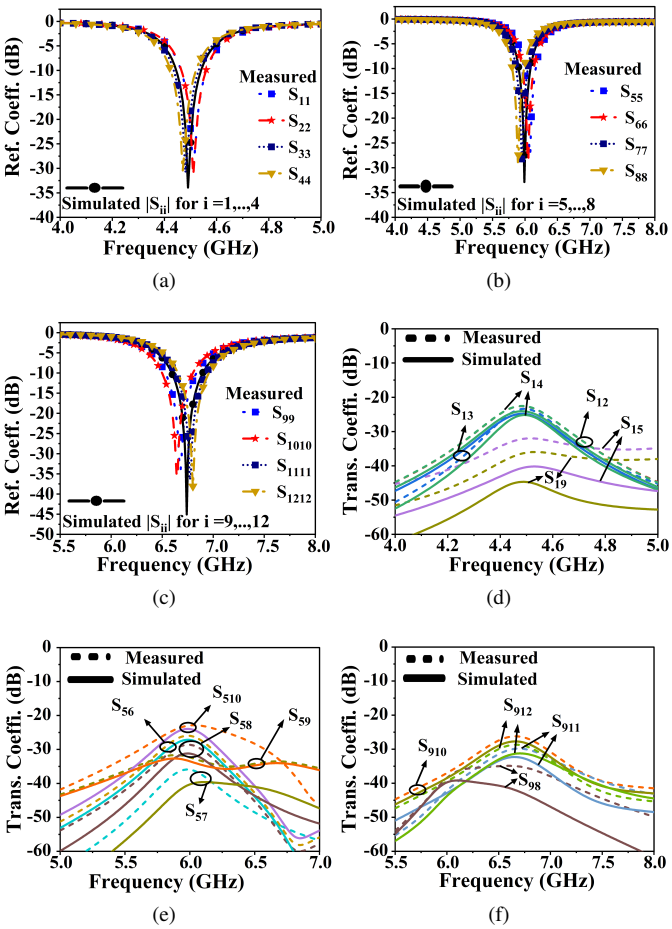

Fig. 12. The measured and simulated results were compared in terms of reflection coefficient for (a) ports 1 to 4, (b) ports 5 to 8, and (c) ports 9 to 12, and transmission coefficient among (d) port 1 to ports 2, 3, 4, 5, and 9, (e) port 5 to ports 6, 7, 8, 9, and 10, and (f) port 9 to ports 8, 10, 11, and 12.

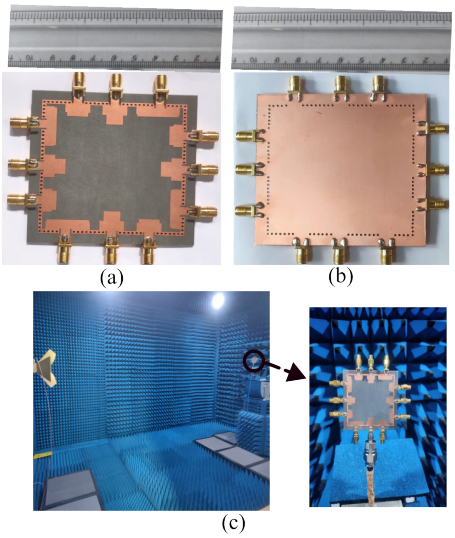

Fig. 13. Images of the fabricated antenna: (a) Top view, (b) Bottom view, and (c) Fabricated prototype in the anechoic chamber.

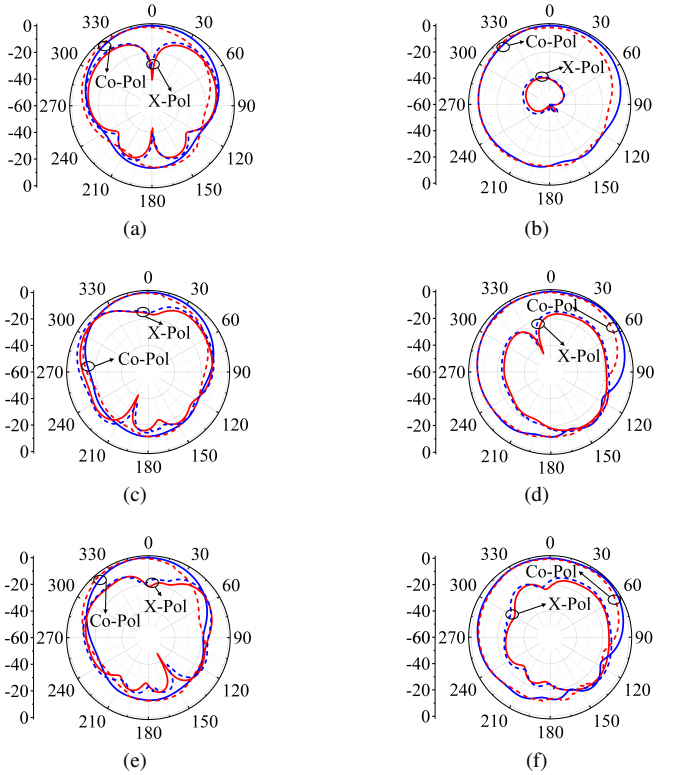

Fig. 14. Radiation pattern at 4.49 GHz (a) ϕ= 0° (E-Plane), (b) ϕ= 90° (H-plane), 6 GHz (c) ϕ= 0° (E-Plane), (d) ϕ= 90° (H-plane), and 6.72 GHz (e) ϕ= 0° (E-Plane), (f) ϕ= 90° (H-plane) [represented by measurement - - - -, simulation ——].

REFERENCES

[1] L. Lu, G. Y. Li, A. L. Swindlehurst, A. Ashikhmin, and R. Zhang, "An Overview of Massive MIMO: Benefits and Challenges," *IEEE Journal of Selected Topics in Signal Processing*, vol. 8, no. 5, pp. 742–758, 2014, doi=10.1109/JSTSP.2014.2317671.

[2] R. Chataut and R. Akl, "Massive MIMO systems for 5G and beyond networks—overview, recent trends, challenges, and future research direction," *Sensors*, vol. 20, no. 10, p. 2753, 2020, https://doi.org/10.3390/s20102753.

[3] E. G. Larsson, O. Edfors, F. Tufvesson, and T. L. Marzetta, "Massive MIMO for next generation wireless systems," *IEEE Communications Magazine*, vol. 52, no. 2, pp. 186–195, 2014, doi=10.1109/MCOM.2014.6736761.

[4] T. L. Marzetta, "Noncooperative Cellular Wireless with Unlimited Numbers of Base Station Antennas," *IEEE Transactions on Wireless Communications*, vol. 9, no. 11, pp. 3590–3600, 2010, doi=10.1109/TWC.2010.092810.091092.

[5] H. Q. Ngo, E. G. Larsson, and T. L. Marzetta, "Energy and Spectral Efficiency of Very Large Multiuser MIMO Systems," *IEEE Transactions on Communications*, vol. 61, no. 4, pp. 1436–1449, 2013, doi=10.1109/TCOMM.2013.020413.110848.

[6] R. S. Kshetrimayum, *Fundamentals of MIMO Wireless Communications*. Cambridge University Press, 2017, https://doi.org/10.1017/9781108234993.

[7] M. Jensen and J. Wallace, "A Review of Antennas and Propagation for MIMO Wireless Communications," *IEEE Transactions on Antennas and Propagation*, vol. 52, no. 11, pp. 2810–2824, 2004, doi=10.1109/TAP.2004.835272.

[8] M. S. Sharawi, "Printed Multi-Band MIMO Antenna Systems and Their Performance Metrics [Wireless Corner]," *IEEE Antennas and Propagation Magazine*, vol. 55, no. 5, pp. 218–232, 2013, doi=10.1109/MAP.2013.6735522.

[9] A. Zanella, N. Bui, A. Castellani, L. Vangelista, and M. Zorzi, "Internet of Things for Smart Cities," *IEEE Internet of Things Journal*, vol. 1, no. 1, pp. 22–32, 2014, doi=10.1109/JIOT.2014.2306328.

[10] L. Chettri and R. Bera, "A Comprehensive Survey on Internet of Things (IoT) Toward 5G Wireless Systems," *IEEE Internet of Things Journal*, vol. 7, no. 1, pp. 16–32, 2020, doi=10.1109/JIOT.2019.2948888.

[11] M.-A. Chung and W.-H. Chang, "Low-cost, low-profile and miniaturized single-plane antenna design for an internet of thing device applications operating in 5G, 4G, V2X, DSRC, WiFi 6 band, WLAN, and WiMAX communication systems," *Microwave and Optical Technology Letters*, vol. 62, no. 04, p. 1765–1773, 2020, https://doi.org/10.1002/mop.32229.
[12] S. K. S. P. P. Singh, P. K. Goswami and G. Goswami, "Frequency reconfigurable multiband antenna for iot applications in WLAN, Wi-MAX, and c-band," *Progress In Electromagnetics Research C*, vol. 102, pp. 149–162, 2020, doi:10.2528/PIERC20022503.
[13] P. Sahoo, P. K. Singhal, and K. Markam, "Enhancing Axial Ratio Bandwidth of Dual Band Microstrip Patch Antenna for GSM Application," *IEEE Latin America Transactions*, vol. 22, no. 4, pp. 352–360, 2024, doi=10.1109/TLA.2024.10472962.
[14] T. Deckmyn, S. Agneessens, A. C. F. Reniers, A. B. Smolders, M. Cauwe, D. Vande Ginste, and H. Rogier, "A Novel 60 GHz Wideband Coupled Half-Mode/Quarter-Mode Substrate Integrated Waveguide Antenna," *IEEE Transactions on Antennas and Propagation*, vol. 65, no. 12, pp. 6915–6926, 2017, doi=10.1109/TAP.2017.2760360.
[15] N. Nguyen-Trong and C. Fumeaux, "Half-Mode Substrate-Integrated Waveguides and Their Applications for Antenna Technology: A Review of the Possibilities for Antenna Design," *IEEE Antennas and Propagation Magazine*, vol. 60, no. 6, pp. 20–31, 2018, doi=10.1109/MAP.2018.2870587.
[16] M. Bozzi, A. Georgiadis, and K. Wu, "Review of Substrate-Integrated Waveguide Circuits and Antennas," *IET Microwaves, Antennas & Propagation*, vol. 5, no. 8, pp. 909–920, 2011, DOI:10.1049/iet-map.2010.0463.
[17] G. Zhai, Z. N. Chen, and X. Qing, "Enhanced Isolation of a Closely Spaced Four-Element MIMO Antenna System using Metamaterial Mushroom," *IEEE Transactions on Antennas and Propagation*, vol. 63, no. 8, pp. 3362–3370, 2015, doi=10.1109/TAP.2015.2434403.
[18] B.-J. Niu and Y.-J. Cao, "Bandwidth-Enhanced Four-Antenna MIMO System Based on SIW Cavity," *Electronics Letters*, vol. 56, no. 13, pp. 643–645, 2020, https://doi.org/10.1049/el.2020.0799.
[19] K. Kumar and S. Dwari, "Compact Four-Element MIMO SIW Cavity Backed Slot Antenna With High Front-to-Back Ratio," *International Journal of RF and Microwave Computer-Aided Engineering*, vol. 29, no. 1, p. e21512, 2019, https://doi.org/10.1002/mmce.21512.
[20] S. Nandi and A. Mohan, "A Compact Eighth-Mode Circular SIW Cavity-Based MIMO Antenna," *IEEE Antennas and Wireless Propagation Letters*, vol. 20, no. 9, pp. 1834–1838, 2021, doi=10.1109/LAWP.2021.3098711.
[21] B.-J. Niu and J.-H. Tan, "Compact SIW Cavity MIMO Antenna with Enhanced Bandwidth And High Isolation," *Electronics Letters*, vol. 55, no. 11, pp. 631–632, 2019, https://doi.org/10.1049/el.2019.0838.
[22] K.-L. Wong, C.-M. Chou, Y.-J. Yang, and K.-Y. Wang, "Multipolarized Wideband Circular Patch Antenna for Fifth-Generation Multi-Input–Multi-Output Access Points Application," *IEEE Antennas and Wireless Propagation Letters*, vol. 18, no. 10, pp. 2184–2188, 2019, doi=10.1109/LAWP.2019.2940032.
[23] K.-L. Wong, H.-J. Chang, J.-Z. Chen, and K.-Y. Wang, "Three Wideband Monopolar Patch Antennas In A Y-Shape Structure for 5G Multi-Input–Multi-Output Access Points," *IEEE Antennas and Wireless Propagation Letters*, vol. 19, no. 3, pp. 393–397, 2020, doi=10.1109/LAWP.2020.2967354.
[24] K.-L. Wong, J.-Z. Chen, and W.-Y. Li, "Four-Port Wideband Annular-Ring Patch Antenna Generating Four Decoupled Waves for 5G Multi-Input–Multi-Output Access Points," *IEEE Transactions on Antennas and Propagation*, vol. 69, no. 5, pp. 2946–2951, 2021, doi=10.1109/TAP.2020.3025237.
[25] I. R. R. Barani, K.-L. Wong, Y.-X. Zhang, and W.-Y. Li, "Low-Profile Wideband Conjoined Open-Slot Antennas Fed by Grounded Coplanar Waveguides for 4×4 5G MIMO Operation," *IEEE Transactions on Antennas and Propagation*, vol. 68, no. 4, pp. 2646–2657, 2020, doi=10.1109/TAP.2019.2957967.
[26] L. Chang and H. Wang, "Miniaturized Wideband Four-Antenna Module Based on Dual-Mode PIFA for 5G 4×4 MIMO Applications," *IEEE Transactions on Antennas and Propagation*, vol. 69, no. 9, pp. 5297–5304, 2021, doi=10.1109/TAP.2021.3069490.
[27] L. Wang and Q. Liao, "Wideband Multibeam SIW Horn Array With High Beam Isolation and Full Azimuth Coverage," *IEEE Transactions on Antennas and Propagation*, vol. 69, no. 9, pp. 6070–6075, 2021, doi=10.1109/TAP.2021.3069564.
[28] K.-L. Wong, T.-C. Wei, Y.-S. Tseng, and W.-Y. Li, "Compact 2×2 Dual-Polarized Patch Antenna Array Transmitting Eight Uncorrelated Waves for the WiFi-6E MIMO Access Point Featuring Eight Spatial Streams," *IEEE Access*, vol. 12, pp. 36 793–36 809, 2024.
[29] K.-L. Wong, H.-C. Kao, and W.-Y. Li, "Wideband Low-Profile Eight-Port Eight-Wave Annular-Ring Patch Antenna Based on Using Eight Dual-Shorted Dual-Resonant Ring Sectors for 8 × 8 MIMO Mobile Devices," *IEEE Access*, vol. 11, pp. 18–32, 2023.
[30] G. Srivastava, A. Kumar, A. Mohan, B. Kumar Kanaujia, L. Matekovits, and I. Peter, "An Eight-Port Frequency Reconfigurable MIMO Antenna Using Liquid Dielectrics," *IEEE Access*, vol. 13, pp. 142 938–142 947, 2025, doi=10.1109/ACCESS.2025.3594828.
[31] S. Yan, P. J. Soh, and G. A. E. Vandenbosch, "Dual-Band Textile MIMO Antenna Based on Substrate-Integrated Waveguide (SIW) Technology," *IEEE Transactions on Antennas and Propagation*, vol. 63, no. 11, pp. 4640–4647, 2015, doi=10.1109/TAP.2015.2477094.
[32] V. S. P. Nayak and K. Manjunathachari, "Design and analysis of the triple band circular quarter mode substrate integrated waveguide (QMSIW) 1 × 2 MIMO antenna," *International Journal of Microwave and Wireless Technologies*, vol. 17, no. 7, p. 1208–1227, 2025, doi=10.1017/S1759078725102286.
[33] S. Priya, K. Kumar, S. Dwari, and M. K. Mandal, "Circularly Polarized Self-Diplexing SIW Cavity Backed Slot Antennas," *IEEE Transactions on Antennas and Propagation*, vol. 68, no. 3, pp. 2387–2392, 2020, doi=10.1109/TAP.2019.2938576.
[34] K. Kumar and S. Dwari, "Substrate Integrated Waveguide Cavity-Backed Self-Triplexing Slot Antenna," *IEEE Antennas and Wireless Propagation Letters*, vol. 16, pp. 3249–3252, 2017, doi=10.1109/LAWP.2017.2771510.
[35] S. Nandi and A. Mohan, "A Self-Diplexing MIMO Antenna for WLAN Applications," *Microwave and Optical Technology Letters*, vol. 61, no. 1, pp. 239–244, 2019, https://doi.org/10.1002/mop.31517.
[36] B. Pramodini, D. Chaturvedi, and G. Rana, "Design and Investigation of Dual-Band 2 × 2 Elements MIMO Antenna-Diplexer Based on Half-Mode SIW," *IEEE Access*, vol. 10, pp. 79 272–79 280, 2022, doi=10.1109/ACCESS.2022.3193253.
[37] A. K. Pandey, R. K. Gangwar, and R. K. Chaudhary, "A Compact SD-QMSIW-Based Self-Diplexing MIMO Antenna Using Two Modified L-Shaped Slots as Radiators for IoT Applications," *IEEE Internet of Things Journal*, pp. 1–1, 2024, doi=10.1109/JIOT.2024.3464590.
[38] B. Pramodini, D. Chaturvedi, L. Darasi, G. Rana, and A. Kumar, "Optimized Compact MIMO Antenna Design: HMSIW-Based and Cavity-Backed for Enhanced Bandwidth," *IEEE Access*, vol. 12, pp. 189 820–189 828, 2024, doi=10.1109/ACCESS.2024.3515101.

Neeraj Gautam (Student Member, IEEE) received the Bachelor of Engineering and the M.Tech. degree in electronics and communication engineering from Rajiv Gandhi Proudyogiki Vishwavidyalaya, Bhopal, India, in 2010 and 2018, respectively. He is pursuing a Ph.D. in electronics and communications engineering from the Dr. SPM IIIT-Naya Raipur, India. His research interests mainly focus on the design and analysis of self-multiplexing SIW antennas and MIMO SIW antennas for 5G antennas and circuits, RF and millimeter wave antennas, IoT networks, and advanced wireless communications. His research work was published in IEEE conferences and reputed journals.

Kundan Kumar (Senior Member, IEEE) received his B. Tech in Electronics and Communication Engineering in 2012, M. Tech and Ph.D. in Electronics and Communication Engineering from Indian Institute of Technology (ISM), Dhanbad, Jharkhand, India in year 2015 and 2020 respectively. Dr. Kumar working as Assistant Professor in the Department of Electronics and Communication Engineering at Dr. B R Ambedkar National Institute of Technology, Jalandhar, Punjab, India. Dr. Kumar has published 20 research papers in referred International Journals (like IEEE Transactions on Antennas and Propagation, IEEE Antennas and Wireless Propagation Letters and etc.) and conferences. He is a regular reviewer of various referred International Journals like IEEE Transactions on Antennas and Propagation, IEEE Antennas and Wireless Propagation Letters and etc. His research interests include 5G antennas and circuits, RF and millimeter wave antennas, intelligent antennas for cognitive radio, characterization of dielectric material, modelling and analysis of substrate-integrated waveguide-based antennas, self-multiplexing antennas, RF planar circuits, RF/microwave sensors, and computational electromagnetics.

Lakhindar Murmu (Member, IEEE) received the B.Tech. degree from the Kalyani Government Engineering College, West Bengal University of Technology, Bidhan Nagar, West Bengal, India, in 2009, the M.E. degree from the Indian Institute of Engineering Science and Technology, Shibpur, India, in 2011, and the Ph.D. degree in microwave engineering from the Indian Institute of Technology (Indian School of Mines), Dhanbad, Jharkhand, India. In 2019, he joined the Dr. Shyama Prasad Mukherjee International Institute of Information Technology, Naya Raipur, India, where he is an assistant professor. He has published several articles in journals and conference proceedings of international repute. His current research interests include planar microstrip antennas, multiband microstrip bandpass filter design, and defected ground structure (DGS) for filter design.

Bipin Chandra Mandi (Senior Member, IEEE) has been continuing as an Associate Professor in the ECE discipline at the International Institute of Information Technology Naya Raipur (IIIT-NR), India, since June 2018. Before joining IIIT-NR, he was an Ad-hoc faculty member at NIT Jamshedpur, Jharkhand, India, in electrical and electronics engineering from November 2016 to May 2018. Dr. Mandi received a B.E. degree in ECE from Bengal Engineering and Science University, Shibpur, India, in 2009, and an M.E. degree in ECE from Jadavpur University, Kolkata, India, in 2011. He received the Ph.D. degree from the Electrical Engineering Department, Indian Institute of Technology, Kharagpur, India, in 2017. His research interests include digital control of DC–DC converters and VLSI implementation.